Research Article

Saeed Alqaed, Jawed Mustafa*, Mohsen Sharifpur*, and Goshtasp Cheraghian*

The effect of graphene nano-powder on the viscosity of water: An experimental study and artificial neural network modeling

https://doi.org/10.1515/ntrev-2022-0155
received February 15, 2022; accepted June 20, 2022

Abstract: Viscosity shifts the flow features of a liquid and affects the consistency of a product, which is a primary factor in demonstrating forces that should be overcome when fluids are transported in pipelines or employed in lubrication. In carbon-based materials, due to their extensive use in industry, finding the simple and reliable equations that can predict the rheological behavior is essential. In this research, the rheological nature of graphene/aqueous nanofluid was examined. Fourier transform infrared spectroscopy, dynamic light scattering, energy-dispersive X-ray spectroscopy, and X-ray powder diffraction were used for analyzing the phase and structure. Transmission electron microscopy and field emission scanning electron microscopy were also employed for micro and nano structural-study. Moreover, nanofluid stability was examined *via* zeta-potential measurement. Results showed that nanofluid has non-Newtonian nature, the same as the power-law form. Further, from 25 to 50°C, at 12.23 s^{-1}, viscosity decreased by 56.9, 54.9, and 38.5% for 1.0, 2.0, and 3.5 mg/mL nanofluids, respectively. From 25 to 50°C, at 122.3 s^{-1}, viscosity decreased by 42.5, 42.3, and 33.3% for 1.0, 2.0, and 3.5 mg/mL nanofluids, respectively. Besides, to determine the viscosity of nanofluid in varied temperatures and mass concentrations, an artificial neural network *via* R^2 = 0.999 was applied. Finally, the simple and reliable equations that can predict the rheological behavior of graphene/water nanofluid are calculated.

Keywords: graphene nano-powder, viscosity, correlation, artificial neural network, flake graphite

1 Introduction

Nanofluids are modern coolants that have been introduced as an alternative to conventional heat transfer fluids and have earned plenty of recognition because of their remarkable thermal characteristics [1–5]. Nanofluids are composed of nanoparticles (NPs) suspended in base fluids, and in fact, the appearance of NPs with a high heat transfer rate has improved the cooling performance of nanofluids [6–8]. So far, many nanofluids have been synthesized, and their thermophysical properties have been measured [9–11]. Also, the cooling performance of these nanofluids in various applications has been investigated both experimentally and numerically [12–16]. It has often been noted that the nanofluids improved heat transfer than conventional coolants; however, it cannot be conclusively said that the general hydrothermal efficiency of nanofluids is better than base fluids [17–19].

Some of the nanofluid applications are enhancement in wear and friction behavior of varied lubricating oils after adding varied nano additives [20]; alumina-titania Therminol-55 hybrid nanofluid is a heat transfer fluid used in concentrating solar collectors [21]; synergism of graphene (G) with titania increase tribological features and provide a greener and efficient lubrication methodology in turning of M2 steel employing a minimum quantity lubrication method [22].

Aside from the many benefits, nanofluids are not without drawbacks. For example, the NPs enhancement in the base fluid enlarges its viscosity, and therefore, the pumping power required for the flow of nanofluids into a

* **Corresponding author: Jawed Mustafa,** Mechanical Engineering Department, College of Engineering, Najran University, P.O. Box (1988), Najran, 61441, Saudi Arabia, e-mail: jmmustafa@nu.edu.sa
* **Corresponding author: Mohsen Sharifpur,** Department of Mechanical and Aeronautical Engineering, University of Pretoria, Hatfield 0028, Pretoria, South Africa; Department of Medical Research, China Medical University Hospital, China Medical University, Taichung 404, Taiwan, e-mail: mohsen.sharifpur@up.ac.za
* **Corresponding author: Goshtasp Cheraghian,** Technische Universität Braunschweig, 38106 Braunschweig, Germany, e-mail: g.cheraghian@tu-braunschweig.de
Saeed Alqaed: Mechanical Engineering Department, College of Engineering, Najran University, P.O. Box (1988), Najran, 61441, Saudi Arabia, e-mail: saalqaed@nu.edu.sa

device is often larger than the base fluid [23]. This increase is sometimes so significant that the general hydrothermal efficiency of nanofluid is poorer than base fluid. In such cases, the use of nanofluids is not recommended at all [24]. Commercial obstacles of nanofluid usage in thermal energy application are detected by Alagumalai *et al.* [25]. According to the before consultation, it could be established that viscosity is one of the highest critical attributes of nanofluids that should be considered. Measurements have shown that many nanofluids are non-Newtonian, meaning that their viscosity at a given temperature is not a fixed number and is a shear rate's (SR) function [26,27]. Considering these types of nanofluids, rheological behavior must be investigated.

Graphene, a carbon-based material, is a two-dimensional form of carbon that contains atoms located in a single layer [28,29]. Graphene has several applications, some of the most important of which are roll-up and wearable electronics, stimulated aside flexibility, energy depository substances, and polymer formation [30].

Gulzar *et al.* [21] experimentally studied the rheological features of Therminol-55-Alumina/TiO_2 nanofluid. They evaluated the influence of nanoparticle mass fraction (0–0.5%) and temperature (20–60°C) on the outcomes. It was depicted that the nanofluid viscosity rises by boosting nanoparticle fraction and temperature reduction. Aghahadi *et al.* [31] experimentally examined the rheological features of engine oil-WO_2-carbon nanotube (CNT) nanofluid. The impact of NPs volume fraction (0–0.6%) and temperature (20–60°C). They developed a mathematical model to determine the rheological features of nanofluid. Esfe and Rostamian [32] experimentally assessed the change in the viscosity of ethylene glycol–CNT/TiO_2 nanofluid *via* SR, temperature, and NPs vol% parameters. The results showed that nanofluid at low concentrations has Newtonian nature, but increasing the vol% leads to the non-Newtonian nature of nanofluid. Kazemi *et al.* [33] tested and compared the rheological nature of aqueous–graphene, water–silica, and water–graphene (30%)/silica (70%) nanofluids. It was revealed that all three nanofluids have non-Newtonian behavior and the most severe non-Newtonian behavior belongs to the water–graphene nanofluid. In an empirical contribution, Ma *et al.* [34] considered the surfactant impact on the rheological behavior of aqueous alumina–CuO and alumina–TiO_2 nanofluids. The considered surfactants were sodium dodecyl sulfate, polyvinyl pyrrolidone, and hexadecyltrimethylammonium bromide. Lee *et al.* [35] explored the temperature impact on the rheological features of carbon-based nanofluids. It was observed that the dynamic viscosity of the examined nanofluid specimen is inferior to the base fluid. While Dalkılıç *et al.* [36] tested the viscosity aspects of water-based silica–graphite hybrid nanofluids, Sekhar and Sharma [37] also Studied the viscosity and specific heat capacity aspects of water-based alumina nanofluids at minimum particle volume fractions. However, Bahrami *et al.* [38] did an empirical research on the rheological manner of hybrid nanofluids made of copper/iron oxide in water/ethylene glycol, whose results revealed a non-Newtonian behavior. Zhao *et al.* [39] did an artificial neural networking (ANN) analysis for entropy/heat generation in the flow of non-Newtonian fluid. Afrand *et al.* [40] also predicted the viscosity of CNTs/water nanofluid by expanding a desirable ANN based on their empirical data. Moreover, Nguyen *et al.* [41] studied the efficiency of joined ANN and genetic algorithms on the impact of concentration/temperature in ethanol-based nanofluid.

In many industrial applications, if there are relationships that can anticipate the nanofluid's thermophysical characteristics with acceptable accuracy, there is no need to measure these properties, which are both time-consuming and costly. This issue has been considered by many researchers, and after measuring the desired property or properties, they have used various techniques to provide an accurate predictive model for that property [42]. One of the methods that have been widely used in the research literature for this mean is the ANN [43,44].

Wahab *et al.* [45] reported an exergy performance of 14.62% gathered at 0.1% volume fraction and 40 L/m by working liquids of water and graphene nanofluid with 0.05–0.15% volume fractions for the hybrid photovoltaic thermal system. Zheng *et al.* [46] experimentally evaluated the rheological manner of ethylene glycol–graphene nanofluid at a temperature range of 5–65°C, the mass fraction of NPs of 0–5%, and SR of (0–90 s^{-1}). Hamze *et al.* [47] investigated shear flow manner of graphene-based nanofluids and also the impact of shearing, and shearing period and temperature on viscosity. Bakhtiari *et al.* [48] examined the readiness of stable titania–graphene/water nanofluids and developed an equation for heat transfer. Nadooshan *et al.* [49] measured the rheological manner of magnetite–CNT/ethylene glycol nanofluid to find heat transfer rate, and the results revealed Newtonian behavior for minimum volume fraction and non-Newtonian behavior for maximum volume fraction. Also, Malekahmadi *et al.* [50] focused on the CNT additive impact on the heat transfer rate of hydroxyapatite/water for dental operations. Shahsavani *et al.* [51] studied the rheological manner of water–EG/functionalized multi walled CNTs.

As for the research gap, the mentioned studies, and other published papers related to the viscosity of carbon-

based materials, did not find the exact correlation for water-based nanofluid containing graphene NPs. Also, the importance of the synthesis process in the viscosity behavior was not mention.

As for the importance, viscosity shifts the flow features of a liquid and affects the consistency of a product; this data is critical in most production steps. Also, viscosity is a primary factor in demonstrating the forces that should be overcome when fluids are transported in pipelines or employed in lubrication. It leads the fluid flow in surface coating, injection molding, and spraying. Viscosity measurement is needed in choosing the antifreeze with minimum viscosity, employed in car engines. Thus, to solve the relevant problems in this regard, we need to measure the viscosity of nanofluids under different conditions, such as SRs, mass concentrations, and temperatures to find the behavior of the fluid. Moreover, we can find out which nanofluid is a better choice for our goal.

As for the key objectives, in the carbon-based materials, especially graphene, due to its extensive use in industry, the exact correlation with the least uncertainty is needed for the scientists to reduce the costs of experiments and the costs in industries. Thus, in this research, after experimental examinations, the numerical study by training ANN models was done to find simple and reliable equations that can predict the rheological manner of water-based nanofluid containing graphene as carbon-based material.

In this study, graphene nanofluid was formed by applying a two-step approach. For this purpose, first, graphene NPs are synthesized by applying the top-down approach. Then, they are dispersed in water at mass concentrations of 1.0–3.5 mg/mL. After preparing the nanofluid samples, their rheological behavior in different mass concentration values and temperatures is measured. Eventually, the ANN technique is selected to obtain a predictive model for the rheological manner of the water–graphene nanofluid.

Table 1: Base fluid and nanoparticle profile table [33,52]

Properties	Graphene–C (Np)	Water–H_2O (Bf)
Molar mass (g/mol)	−12.0	−18.0
Density (g/m^3)	−2.16	0.997
Boiling point (°C)	4200.0	100.0
Melting point (°C)	3670.0	0.0

2 Materials and methods

2.1 Materials

From KaraPA-Iran, graphite in flake form was prepared at 99.8% purity. Moreover, additional materials consumed in the synthesis had purity above 99% and was of analytical grade. Figure 1 displays G/flake graphite (FG) three-dimensional structure design. Further, base fluid and nanomaterial properties are shown in Table 1.

2.2 Methods

2.2.1 Solid/nanofluid formation

Figure 2 shows graphene powder and nanofluid synthesis and preparation steps. Graphene could be produced by

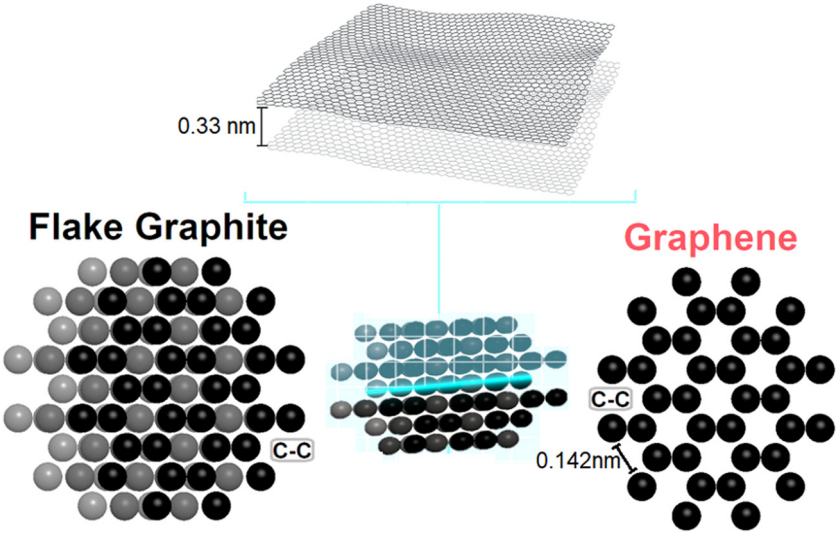

Figure 1: 3D-schematic design of graphene and flake graphite.

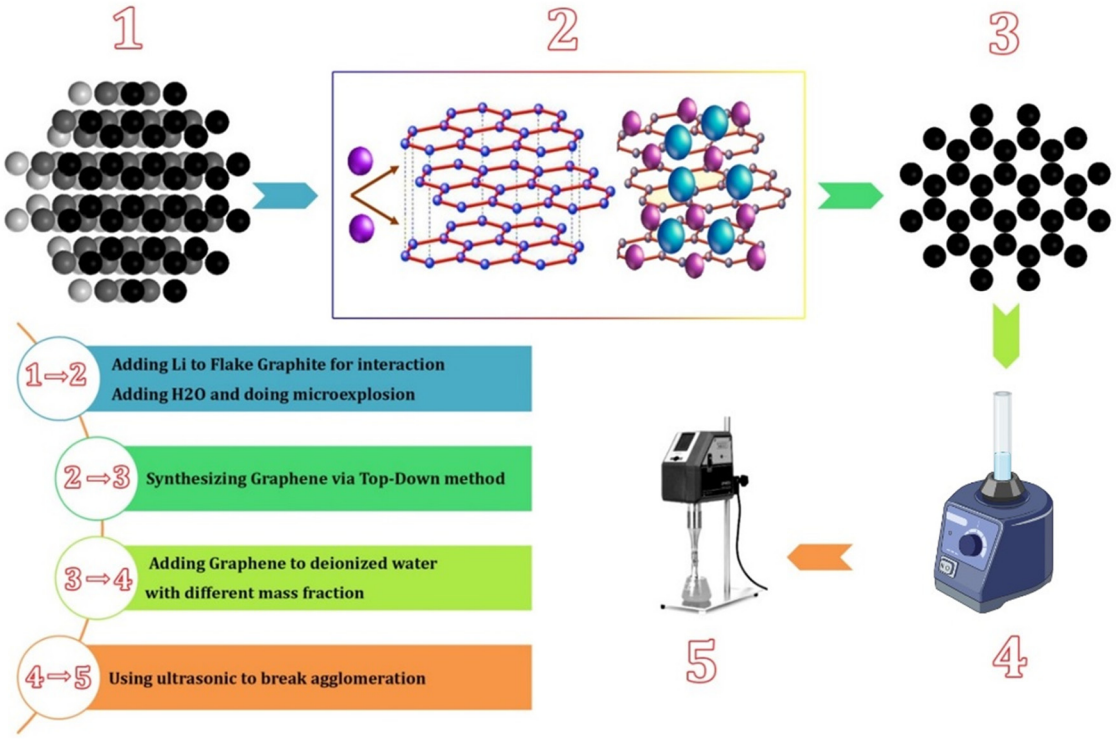

Figure 2: Synthesis steps of powder (schematic diagram from flake graphite to graphene) and preparation steps of nanofluid.

exfoliation of bulk graphite containing direct liquid-phase exfoliation of FG/FG intercalation compound aside from the help of ultrasonication (Figure 2). Lithium is the lightest solid/metal element. In Figure 2, in steps 1 to 2, lithium is employed to be placed between graphite sheets. This helps the micro-explosion between graphite sheets by adding H_2O. Further, in steps 2 to 3, when the micro-explosion is completed, the mono-layer sheets of graphene are obtained.

X-ray diffraction (XRD) was examined *via* a D8 ADVANCE X-ray diffractometer (Bruker-USA). Moreover, to prove XRD results, energy-dispersive X-ray spectroscopy (EDX) was used. Further, dynamic light scattering (DLS) was tested by a VASCO NP size analyzer (Cordouan Technologies, France). Also, Fourier transform infrared spectroscopy (FTIR) spectra was reported using FP-6300 (JASCO, JAPAN). Then, to detect sample morphology, field emission scanning electron microscopy (FESEM) was used (Nova NanoSEM 450; FEI, USA) [51].

To measure the thermophysical properties, nanofluid must be prepared first. Graphene must be added to deionized water. Overall mass concentration of graphene consumed in nanofluid can be calculated *via* equation (1). First, graphene mass is determined *via* weighing balance in the laboratory, and then the two-stage process is used to prepare the nanofluid. Nanofluids were prepared at mass concentrations of 1.0, 1.5, 2.0, 2.5, 3.5 mg/mL. In this method, NPs are mixed in base fluid *via* an appropriate dispersion method, but here, agglomeration is the biggest problem. To achieve good dispersion and avoid agglomeration, 90 min of magnetic stirring and 30 min of sonication are performed *via* 400 W, 24 kHz UP400St Ultrasonicator (Hielscher, Germany) to prepare a stable suspension [36].

$$\phi = \left[\frac{\left(\frac{w}{\rho}\right)_{G}}{\left(\frac{w}{\rho}\right)_{G} + \left(\frac{w}{\rho}\right)_{\text{Water}}} \right] * 100. \quad (1)$$

where mass fraction percentage and density are denoted by φ and ρ, respectively. Mass is indicated by "m."

2.3 Viscosity measurement

In this research, *via* DV2T viscometer (AMETEK Brookfield, USA), G-distilled water (DW) rheological behavior was determined with 5% uncertainty [52,53]. LV spindle (1–6 MPa s/1–200 RPM) is used to measure rheological behavior [53]. Initially, at room temperature, DV2T was scaled *via* DW. For every rheological behavior study, tests were repeated 3 times for 25–50°C temperatures at different SRs, independently [54].

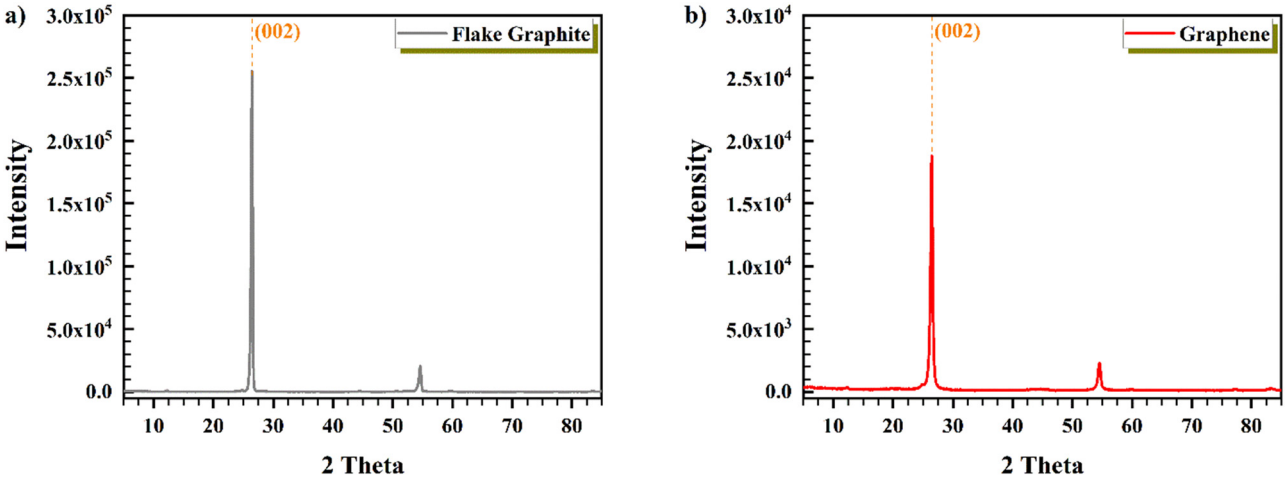

Figure 3: XRD pattern of (a) flake graphite and (b) graphene.

3 Result and discussion

3.1 Solid formation

3.1.1 Structural/phase study

3.1.1.1 X-Ray diffraction

Figure 3 shows the XRD spectra for FG and graphene with a peaked point in (002) surface at 2θ = 26.469°. Low-intensity peaks and (002)-main peak were displayed in the pattern. *D*-spacing was around 3.362 Å for FG and around 3.363 Å for graphene (Bragg's law) [55].

3.1.1.2 DLS

Size distribution for graphite and graphene (water dispersion) was determined by DLS. Graphene has a two-dimensional structure, and a dimension is at the nanoscale. Nevertheless, DLS measured the size of two other dimensions (which are in microscale) alongside its thickness. Figure 4 displays that graphene (49.49 vol% at 76.196 nm and 72.66 vol% at 311.21 nm) has fewer vol% compared to the flake graphite (39.48 vol% at 653.488 nm) [56]. Since graphene has only one dimension in the nanoscale, it is logical that two other dimensions which are in the microscale affect the outcome of DLS and increase the size by more than 100 nm. However, the obtained results also showed that those two dimensions are less than 400 nm which is acceptable.

3.1.1.3 FTIR

FTIR spectroscopy was used to study the FG and graphene structure alongside the functional groups. A large peak from 3,000 to 3,732 cm^{-1} shown in Figure 5 in a large-frequency field is related to the O–H groups of molecules of water for graphene. Likewise, C=C unique

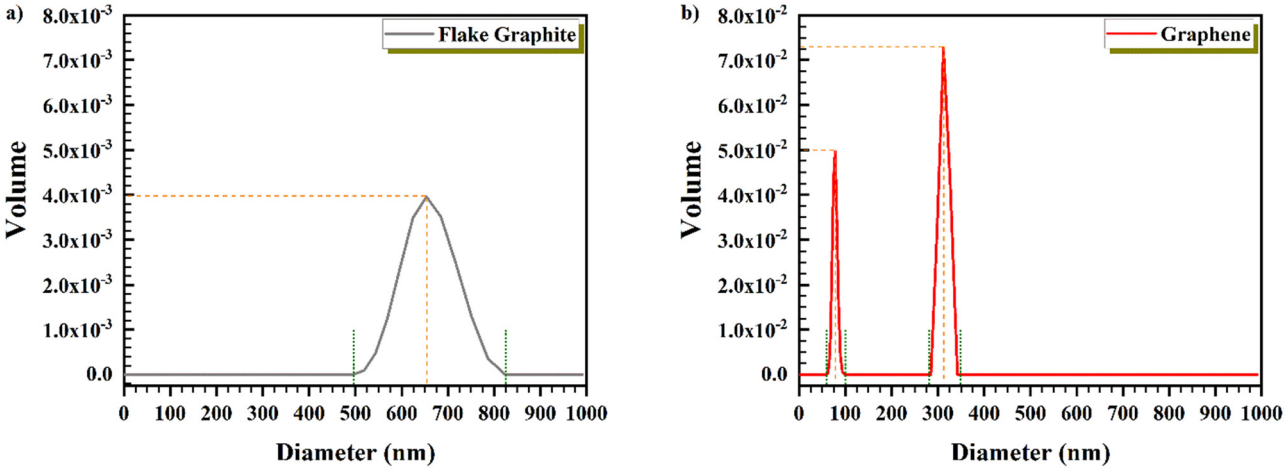

Figure 4: DLS of (a) flake graphite and (b) graphene.

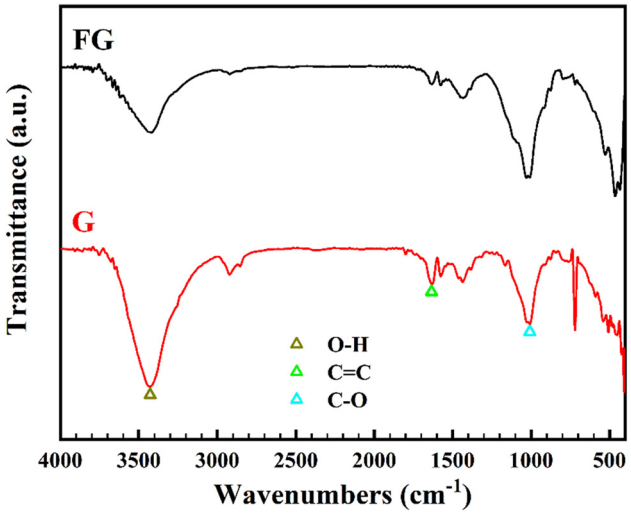

Figure 5: FTIR for graphene and flake graphite.

peak is shown in 1634.38 cm^{-1}. FG and graphene FTIR in Figure 5, showed that the O–H peak domain has less depth for FG. Aromatic C=C group point at 1624.64 cm^{-1} in the FG and at 1634.38 cm^{-1} in graphene. For the FG specimen, C–O has higher intensity (1008.59 cm^{-1} for G and 1010.99 cm^{-1} for FG) [57].

3.1.2 Micro-nano formative study

3.1.2.1 FESEM and EDX analyzer

FESEM image of amorphous and disordered two-dimensional graphene is shown in Figure 6 [58]. Graphene thickness is lesser than 100 nm with layer structure. In graphene, folded sections are on top of each other. Flake diameter for graphene layers is reported as 0.5–3.5 µm [58]. Hence, the morphology approved DLS results and showed that all of

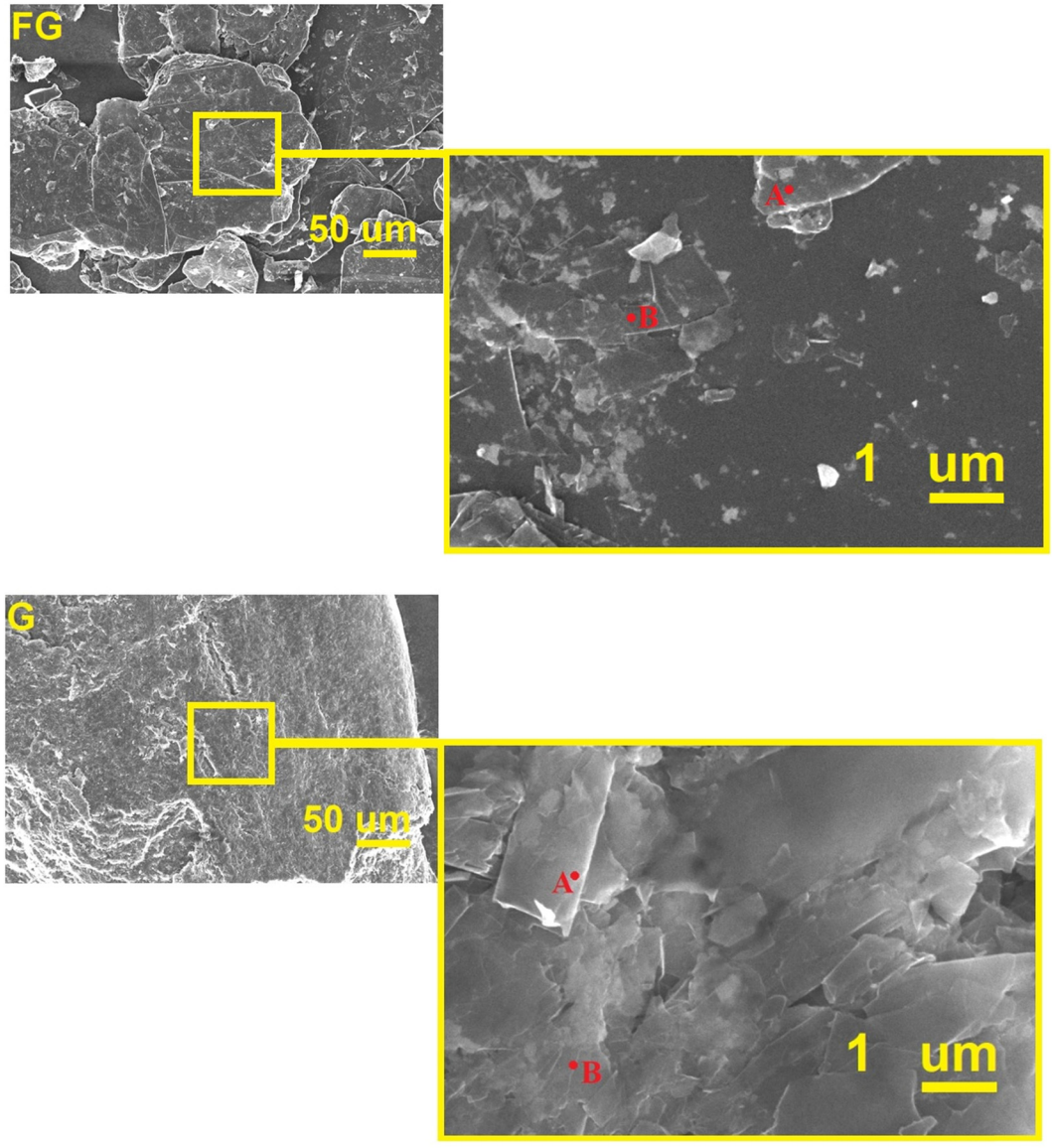

Figure 6: FESEM image for graphene and flake graphite.

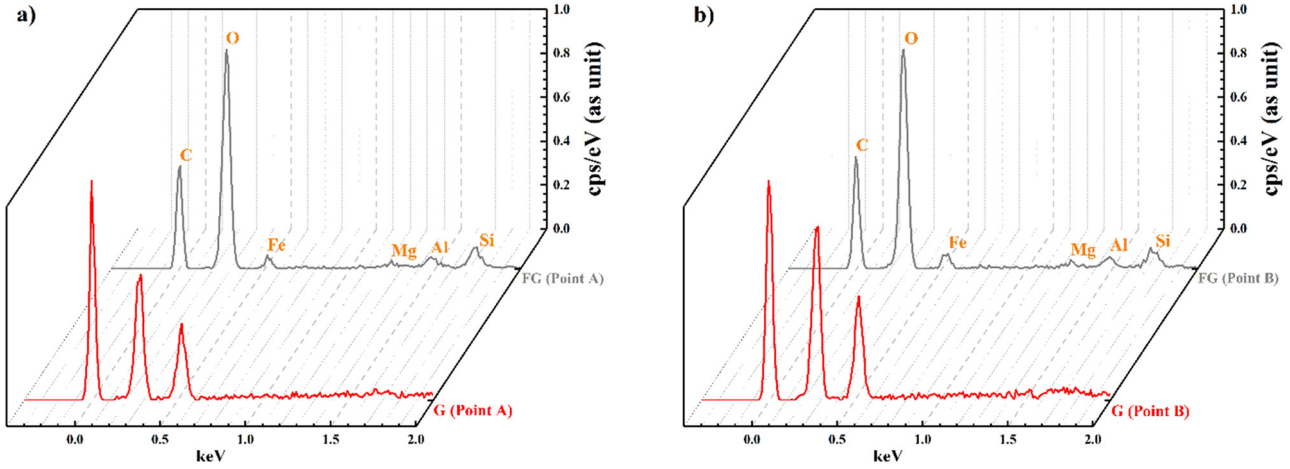

Figure 7: EDX pattern of flake graphite and graphene for (a) point A and (b) point B.

the dimensions of graphene are less than 400 nm. Also, the one dimension of graphene which is in the nanoscale has less than 100 nm thickness. Two points energy dispersive X-ray spectroscopy examined for graphite and graphene. Figure 7 and Table 2 show that FG has about 90.48 at% C, 7.29 at% O, and 2.23 at% Si + N + Al. Nevertheless, graphene is pure at 100 at% C.

3.1.2.2 Transmission electron microscopy (TEM)

To support that graphene thickness is below 100 nm, TEM was used. For image-making in the TEM method, the electron beam was transferred thru a sample. Figure 8 shows that graphene thickness is lesser than 40 nm with a two-dimensional layer structure [58]. These results were also consistent with that of DLS and FESEM. As can be seen, the thickness of graphene is less than 100 nm.

3.2 Nanofluids formation

3.2.1 Stability of nanofluid

3.2.1.1 Zeta potential

The zeta potential (ZP) of graphene is shown in Figure 9 at mass concentrations of 4.5 and 1.0 mg/mL. The colloid mixture of graphene liquid at the 2–4 pH range shows negative ZP. As announced *via* ASTM, the absolute zeta potential of 20–30 mV are rather stable, and >±30 mV is extremely stable. ZPs for 1.0 mg/mL, are −28.8 mV (electrophoretic mobility [EM] of −0.000229 cm^2/Vs) and −27.3 mV (EM of −0.000214 cm^2/Vs), while for 4.5 mg/mL, are −25.7 (EM of −0.000190 cm^2/Vs) and −19.7 (EM of −0.000178 cm^2/Vs). These amounts show nanomaterial's moderate stability in water. It can be seen by these values that by increasing the mass concentration, graphene has aggregation behavior [59,60].

Table 2: EDX elemental composition for flake graphite and graphene

Flake graphite – point A					Graphene – point A				
El AN series unn. C norm. C atom. C error (1 Sigma)					El AN series unn. C norm. C atom. C error (1 Sigma)				
	[wt%]	[wt%]	[at%]	[wt%]		[wt%]	[wt%]	[at%]	[wt%]
C	86.78	86.78	90.48	14.29	C	97.97	97.97	98.38	16.70
O	9.32	9.32	7.29	4.14	O	1.26	1.26	0.95	1.84
Si	1.78	1.78	0.79	0.16	N	0.77	0.77	0.67	2.34
Al	1.08	1.08	0.50	0.13					
N	1.04	1.04	0.94	1.95					
Total	100	100	100			100	100	100	
Flake graphite – point B					**Graphene – point B**				
El AN series unn. C norm. C atom. C error (1 Sigma)					El AN series unn. C norm. C atom. C error (1 Sigma)				
	[wt%]	[wt%]	[at%]	[wt%]		[wt%]	[wt%]	[at%]	[wt%]
C	100.00	100.00	100.00	16.47	C	100.00	100.00	100.00	17.05
Total	100	100	100			100	100	100	

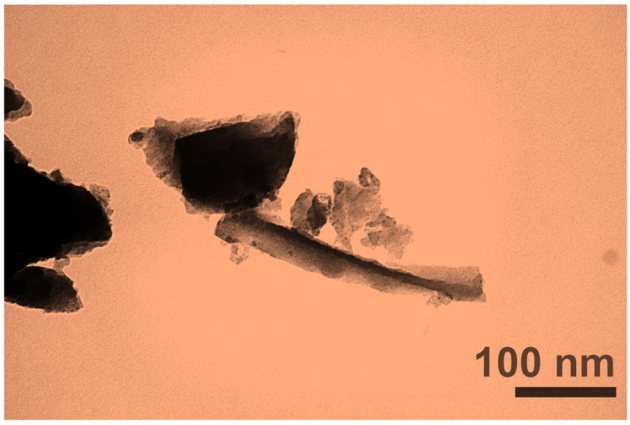

Figure 8: TEM of graphene.

3.2.2 Rheological behavior study

3.2.2.1 Validation

DV2T apparatus validity was determined and related to the ASHRAE handbook [53] to affirm the apparatus correctness. Regarding manual, apparatus uncertainty was satisfying (lesser that 5%) at T = 25°C. Figure 10 displays the maximum error of 4.29% (at T = 40°C) [53].

3.2.2.2 Mass concentration and temperature effect

An important stage in determining the nanofluid's viscosity is to measure it at different mass concentrations and temperatures, to determine whether it exhibits Newtonian/non-Newtonian behavior [61]. For varied temperatures, Figure 11 exhibits viscosity corresponding to mass concentration in 12.23 and 122.3 SRs [62]. At different mass concentrations, Figure 12 exhibits viscosity corresponding to temperature in

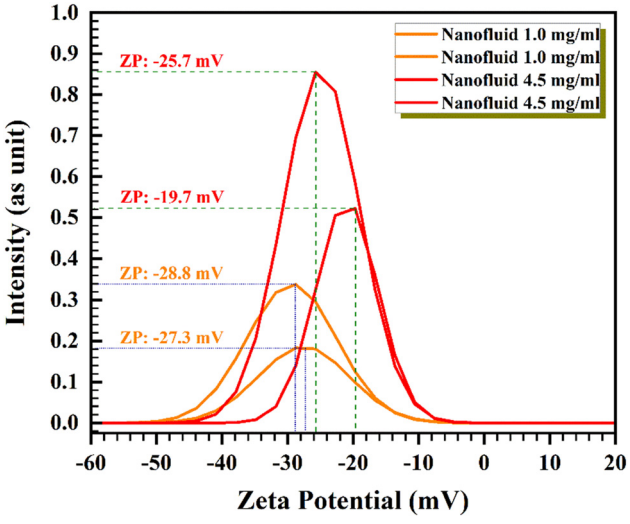

Figure 9: ZP pattern of graphene at mass concentrations of 1 and 4.5 mg/mL.

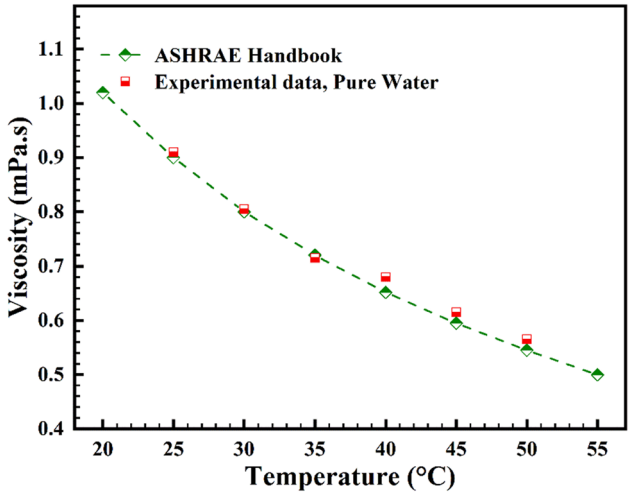

Figure 10: Viscosity vs distilled water temperature compared to that in ASHRAE handbook [53].

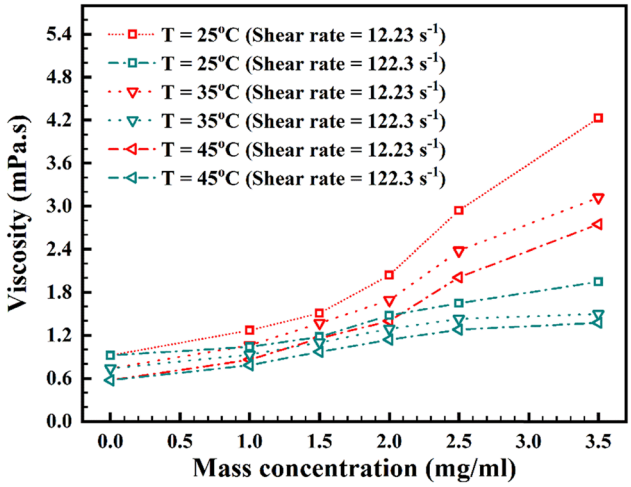

Figure 11: Change in rheological behavior corresponding to mass concentration at varied temperatures.

12.23 and 122.3 s^{-1} SRs [63]. On increasing the mass concentration and temperature, there is an increase and decrease in viscosity, respectively. As can be seen, in the 12.23 s^{-1} SR, from mass concentration of 0.0 to 2.0 mg/mL, the viscosity increment is relatively smooth; but after 2.0–3.5 mg/mL, the enhancement of viscosity is more steep. This is due to the surface tension increment at low speed for the agglomerations. However, this slope increment cannot be seen in the 122.3 s^{-1} SR, which reveals that with speed increment, the agglomerations are broken, and thus, the friction is decreased. Also, temperature increment causes a decrement in agglomerations, and again, friction is decreased at 45°C.

Figure 13 exhibits the rheological behavior 3D data corresponding to various mass concentrations and

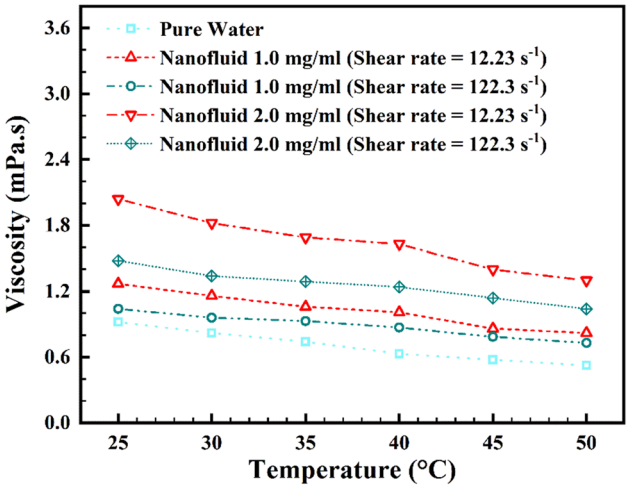

Figure 12: Change in rheological behavior corresponding to temperature at varied mass concentrations.

temperatures from 122.3–12.23 SRs [64]. Viscosity at varied mass concentrations and temperatures is reported in Table 3. As can be seen, with temperature enhancement, there was a decrease in viscosity. Also, the addition of graphene caused an enhancement in viscosity. The viscosity trend is dependent on two variables, temperature and concentration. However, these variables have a different effect on viscosity. To find which one has greater impact, first, a comparison between the minimum and maximum values is needed.

When the temperature is constant, the mass concentration impact can be measured. For 25°C which is in the room-temperature domain, viscosity for 1.0 mg/mL graphene was 1.27 MPa s (12.23 s^{-1} SR) and 1.04 MPa s (122.3 s^{-1} SR), while it reached to 2.04 MPa s (12.23 s^{-1} SR) and 1.48 MPa s (122.3 s^{-1} SR) for 2.0 mg/mL graphene, then it reached to 4.23 MPa s (12.23 s^{-1} SR) and 1.95 MPa s (122.3 s^{-1} SR) for 3.5 mg/mL graphene. This means by adding more graphene, from 1.0 to 3.5 mg/mL, viscosity increment was 233.07% (12.23 s^{-1} SR) and 87.50% (122.3 s^{-1} SR).

For 50°C, which is in the heating domain, viscosity for 1.0 mg/mL graphene was 0.82 MPa s (12.23 s^{-1} SR) and 0.73 MPa s (122.3 s^{-1} SR), while it reached to 1.30 MPa s (12.23 s^{-1} SR) and 1.04 MPa s (122.3 s^{-1} SR) for 2.0 mg/mL graphene, then it reached to 2.60 MPa s (12.23 s^{-1} SR) and 1.30 MPa s (122.3 s^{-1} SR) for 3.5 mg/mL graphene. This means by adding more graphene, from 1.0 to 3.5 mg/mL, viscosity increment was 217.07% (12.23 s^{-1} SR) and 78.08% (122.3 s^{-1} SR).

When the mass concentration is constant, the temperature impact can be measured. For 1.0 mg/mL graphene/water nanofluid, viscosity at 25°C was 1.27 MPa s (12.23 s^{-1} SR) and 1.04 MPa s (122.3 s^{-1} SR), while it decreased to 0.82 MPa s (12.23 s^{-1} SR) and 0.73 MPa s (122.3 s^{-1} SR) on increasing the temperature to 50°C. This means by increasing the temperature, and on reaching the heating domain, from 25–50°C, viscosity decrement was 35.43% (12.23 s^{-1} SR) and 29.81% (122.3 s^{-1} SR).

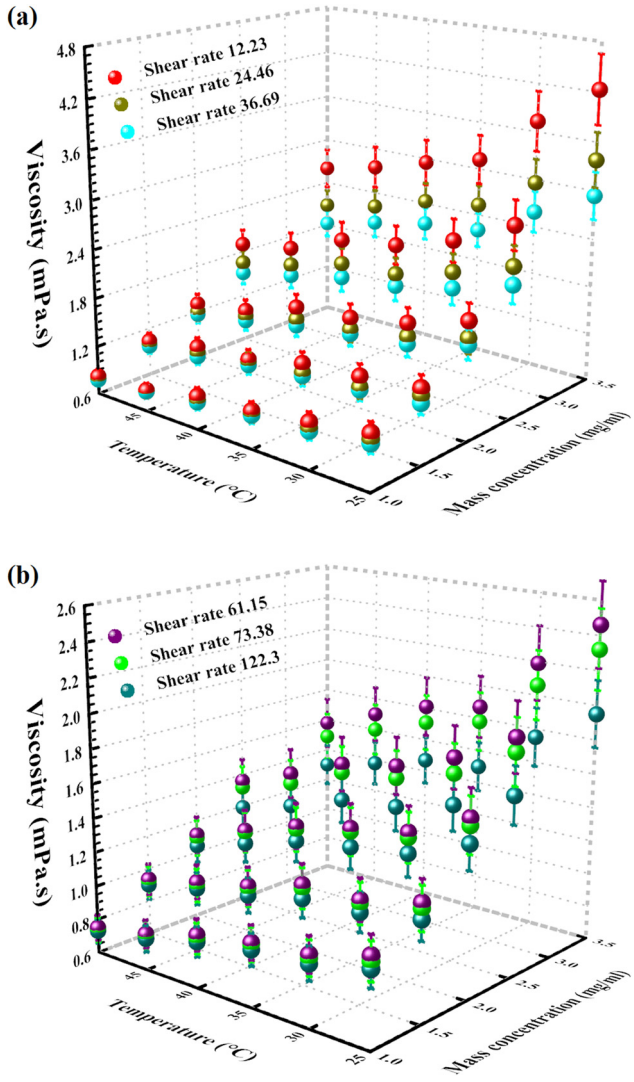

Figure 13: The 3D factual outcome of viscosity at dissimilar temperatures and mass concentrations.

Table 3: Viscosity at varied temperatures and mass concentrations

Shear rate (s^{-1})	T = 25°C (MPa s)	T = 50°C (MPa s)
	Nanofluid 1.0 mg/mL	
12.23	1.27	0.82
122.3	1.04	0.73
	Nanofluid 2.0 mg/mL	
12.23	2.04	1.30
122.3	1.48	1.04
	Nanofluid 3.5 mg/mL	
12.23	4.23	2.60
122.3	1.95	1.30

For 2.0 mg/mL graphene/water nanofluid, viscosity at 25°C was 2.04 MPa s (12.23 s^{-1} SR) and 1.48 MPa s (122.3 s^{-1} SR), while it decreased to 1.30 MPa s (12.23 s^{-1} SR) and 1.04 MPa s (122.3 s^{-1} SR) on increasing the temperature to 50°C. This means by increasing the temperature, and on reaching the heating domain, from 25–50°C, viscosity decrement was 36.27% (12.23 s^{-1} SR) and 29.73% (122.3 s^{-1} shear rate).

For 3.5 mg/mL graphene/water nanofluid, viscosity at 25°C was 4.23 MPa s (12.23 s^{-1} SR) and 1.95 MPa s (122.3 s^{-1} SR), while it decreased to 2.60 MPa s (12.23 s^{-1} SR) and 1.30 MPa s (122.3 s^{-1} SR) on increasing the temperature to

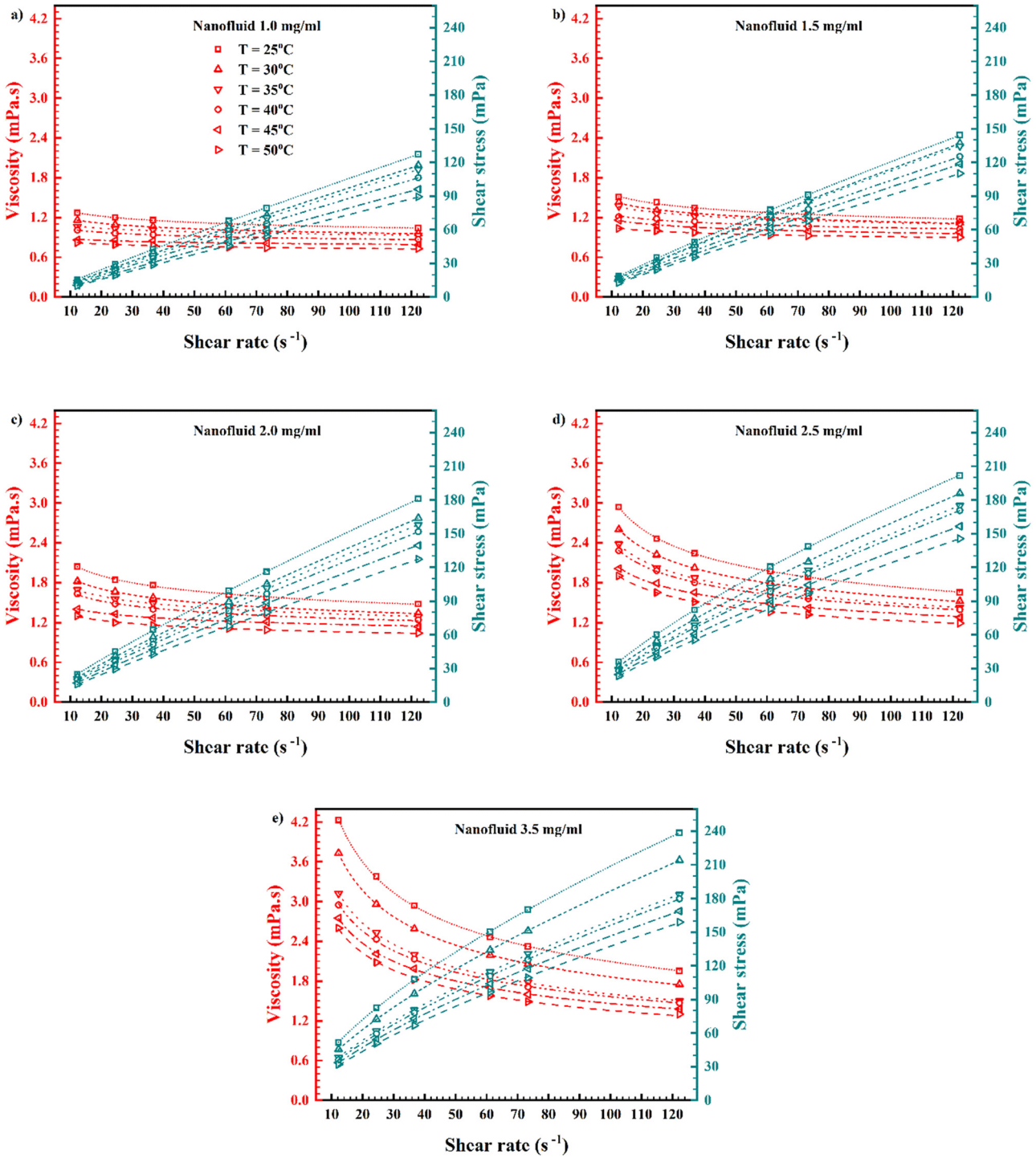

Figure 14: Viscosity and shear stress values against SR for different mass concentrations and temperatures.

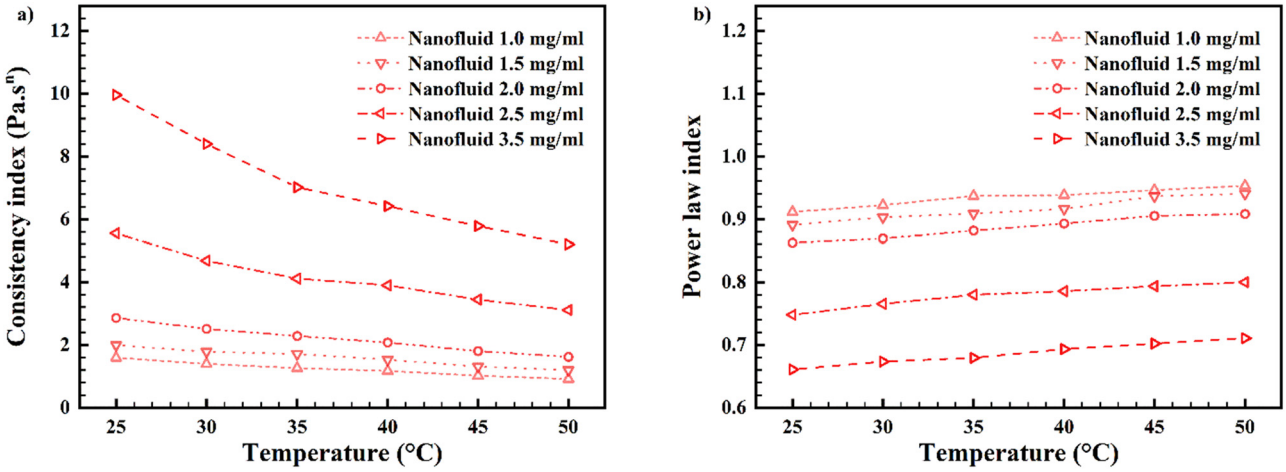

Figure 15: Consistency index "*m*" (a) and power-law index "*n*" (b) against temperature for various mass concentrations.

50°C. This means that by increasing the temperature and on reaching the a heating domain, from 25°C–50°C, viscosity decrement was 38.53% (12.23 s^{-1} SR) and 33.33% (122.3 s^{-1} SR). This means that temperature caused a decrement in viscosity; however, in 3.5 mg/mL graphene, this decrement was more. Further, the rheological behavior of water became as non-Newtonian after adding graphene to water.

3.2.2.3 Non-Newtonian behavior

Figure 14 displays the viscosity–shear stress (SS) of nanofluid corresponding to SR for temperatures of 25–50°C and mass concentrations of 1.0–3.5 mg/mL. Nanofluid's rheological behavior indicated a non-Newtonian manner. Categorizations for non-Newtonian manner are time self-reliant (shear thinning/shear thickening) and time reliant [65]. In G–DW, power is less than one (in the equation of power-law), which causes the shear-thinning (pseudo-plastic) [66]. Power law:

$$\tau = m\dot{\Upsilon}^{n}, \tag{2}$$

where n (dimensionless) is the power law index, m (Pa S^n) is the flow consistency index, and τ(Pa) denotes SS, and $\dot{\Upsilon}$ (s^{-1}) denotes shear rate.

Hence, equation (3) estimates the viscosity:

$$\mu = m\dot{\Upsilon}^{n-1}, \tag{3}$$

where "μ" denotes viscosity [67].

The trend for viscosity – SS by SR is non-linear. Therefore, concluding based on the patterns, SS is a variable of temperature and mass concentration. Hence, n or m with varied temperature or mass concentration could be estimated using curve-fitting plus equation (4).

$$\tau = \mu\dot{\Upsilon}. \tag{4}$$

In Figure 15, m (consistency index) and n (power-law index) variations are made known concerning nanofluid's non-Newtonian nature and Figure 14 data. Figure 15a exhibits consistency index; in conclusion, mass concentration increment caused the "m" increment, but temperature increment for each wt% caused the "m" decrement [68]. Figure 15b exhibits power-law index (n); in conclusion, mass concentration increment caused the "n" decrement, but temperature increment for each wt% caused the "n" increment [69]. This happened because the viscosity decreased after temperature increment, which caused the nanofluid to act the same way as the Newtonian nature of DW base fluid.

3.2.3 Statistical view

3.2.3.1 Recommended equation

G–DW nanofluid correlation is recommended for estimating viscosity *via* curve-fitting (equations (5)–(10)). These correlations have $R^2 \sim 0.99$ [70]. Three-dimensional fitted correlation on empirical input of 12.23–122.3 SRs is displayed in Figure 16.

$$\text{Viscosity}_{12.23} = (1.13936)\star((T/T_0)^{(-0.66909)}) \star(wt^{(1.01453)}). \tag{5}$$

Reduced Chi-Square: 0.00622, R^2 (**Coefficient of determination**): 0.99687, and **adjusted** R^2: 0.99664,

$$\text{Viscosity}_{24.46} = (1.11064)\star((T/T_0)^{(-0.61507)}) \star(wt^{(0.85601)}). \tag{6}$$

Reduced Chi-Square: 0.00909, R^2: 0.97995, and **adjusted** R^2: 0.97847,

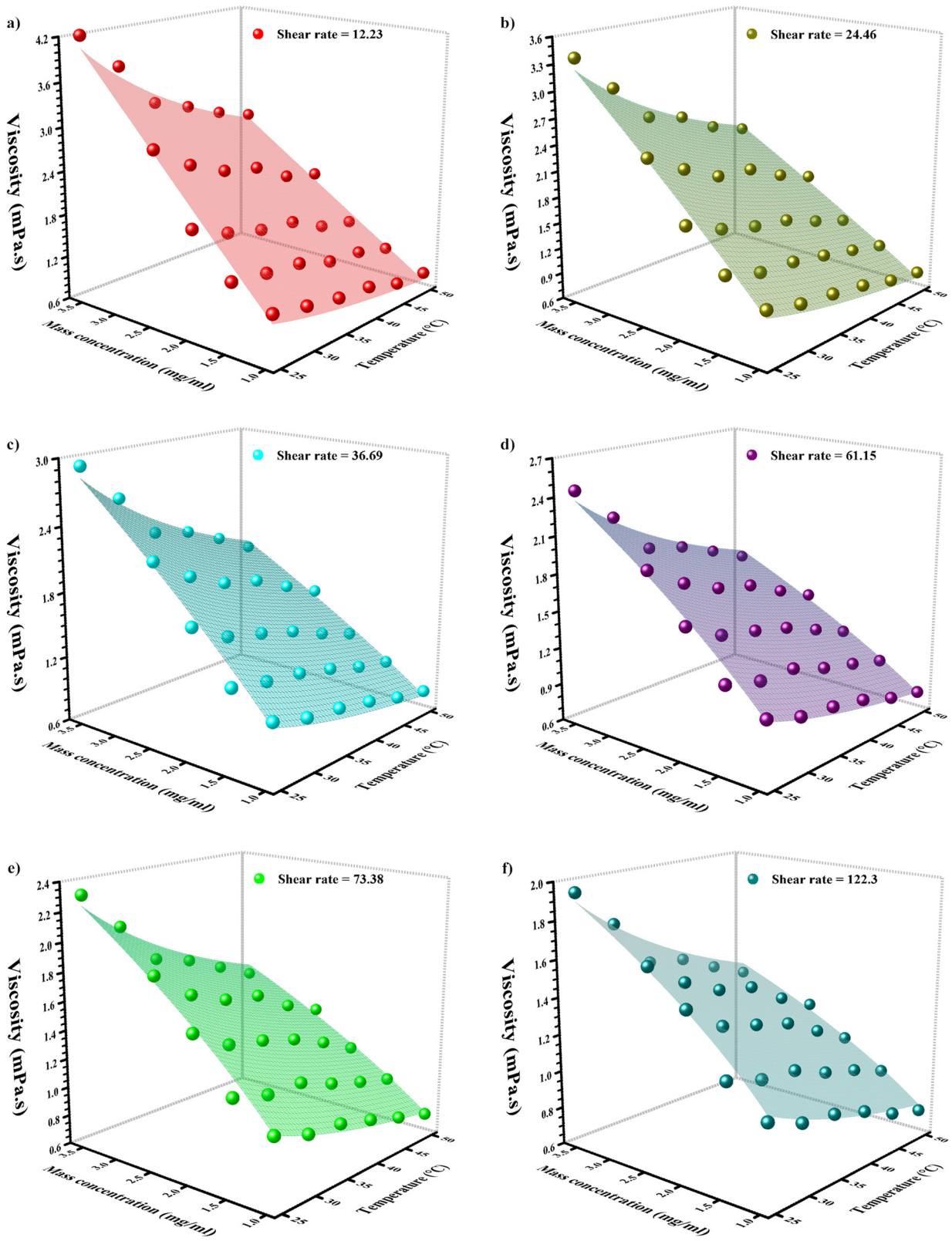

Figure 16: Confirmation of recommended correlation with original measurements; Viscosity *via* mass concentration and nanofluid temperature for varied SRs.

$$\text{Viscosity}_{36.69} = (1.11072)\star((T/T_0)^{(-0.58931)}) \star(wt^{(0.74706)}). \quad (7)$$

Reduced Chi-Square: 0.00616, R^2: 0.98006, and **adjusted R^2-Square:** 0.97859,

$$\text{Viscosity}_{61.15} = (1.09064)\star((T/T_0)^{(-0.54171)}) \star(wt^{(0.62346)}). \quad (8)$$

Reduced Chi-Square: 0.00362, R^2: 0.98062, and **adjusted R^2**: 0.97918,

$$\text{Viscosity}_{73.38} = (1.08272)\star((T/T_0)^{(-0.52778)}) \star(wt^{(0.58263)}). \quad (9)$$

Reduced Chi-Square: 0.00323, R^2: 0.97934, and **adjusted R^2**: 0.97781,

$$\text{Viscosity}_{122.3} = (1.07025)\star((T/T_0)^{(-0.49058)}) \star(wt^{(0.45972)}). \quad (10)$$

Reduced Chi-Square: 0.0019, R^2: 0.99872, and **adjusted R^2**: 0.99863,

where "T" and "wt" are temperature and mass concentration, respectively, and "T_0" is 25°C, and viscosity is in centipoise [71].

The recommended equation could be confirmed by the original viscosity information. Equation (11) is employed to correlate deviation. The highest deviation of margin exhibited in Figure 17, which quantified 1.8% (for 10 RPM) and 0.96% (for 100 RPM), exhibits such original equation with significant accuracy [71].

$$\text{Dev} = \left[\frac{\mu_{\text{Exp}} - \mu_{\text{Pred}}}{\mu_{\text{Pred}}}\right] \star 100. \quad (11)$$

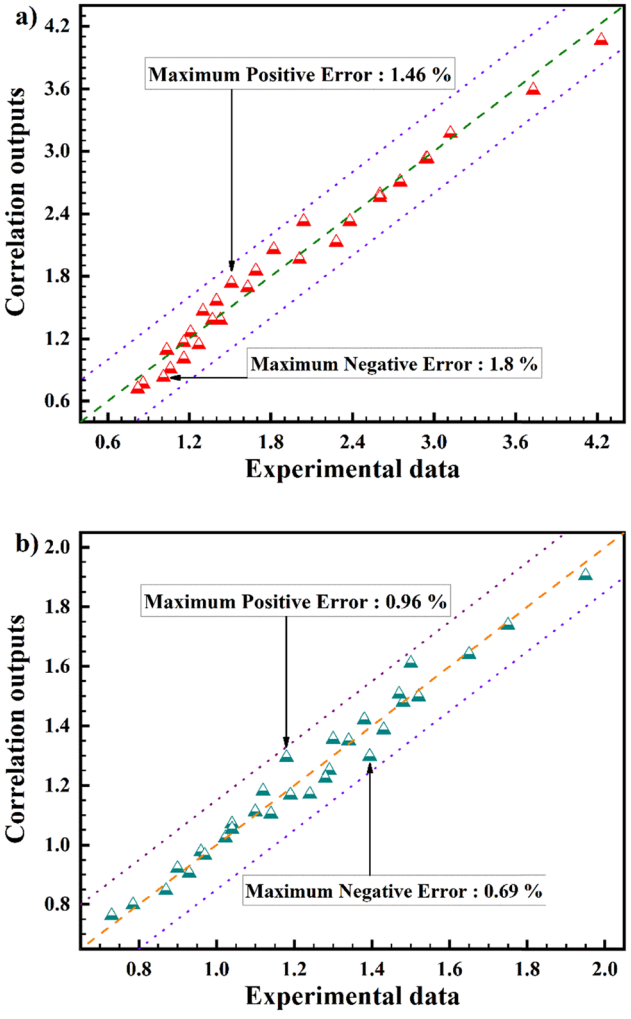

Figure 17: Affirmation of original correlation with from factual data for (a) 10 RPM and (b) 100 RPM.

3.2.3.2 ANN

In this study, viscosity for each SR (12.23, 24.46, 36.69, 61.15, 73.38, and 122.3 s^{-1}), in 5 mass concentrations (1.0, 1.5, 2.0, 2.5, and 3.5 mg/mL), and 6 temperatures (25, 30, 35, 40, 45, and 50°C) were measured. This means that for each SR, 30 data (5 mass concentrations for 6 temperatures) were measured. However, the gap between the measured values is unknown.

To cut down the data-gathering cost and to find all the data for each mass concentration or temperature, ANN modeling was done with an acceptable margin of deviation. Thus, any researcher who wants to calculate the viscosity of graphene/water at any mass concentration or temperature can use the original equations in this study.

Graphene viscosity was modeled in this study. There are three inputs for this model: SR, mass concentration, and temperature. Also, Output for this model is viscosity [71]. Thus, an ANN was applied. ANN has the output and hidden layers. The output layer has a linear transfer function, while 16 sigmoid neurons are in the hidden layer. For the training algorithm, the Bayesian regularization backpropagation is engaged [72–74]. A model trained for 122.3–12.23 (1/s). Figure 18 displays the main data contour as dashed lines, while the trained data contour is shown as solid lines. It is noticeable that SR critically affects foretoken viscosity. Further, it is detected that viscosity increases with mass concentration increment. However, it decreases with the temperature increment. Also, mass concentration has a major impact [75–77]. ANN is successful in predicting behaviors of the nanofluid stand on viscosity's analytical variations, which

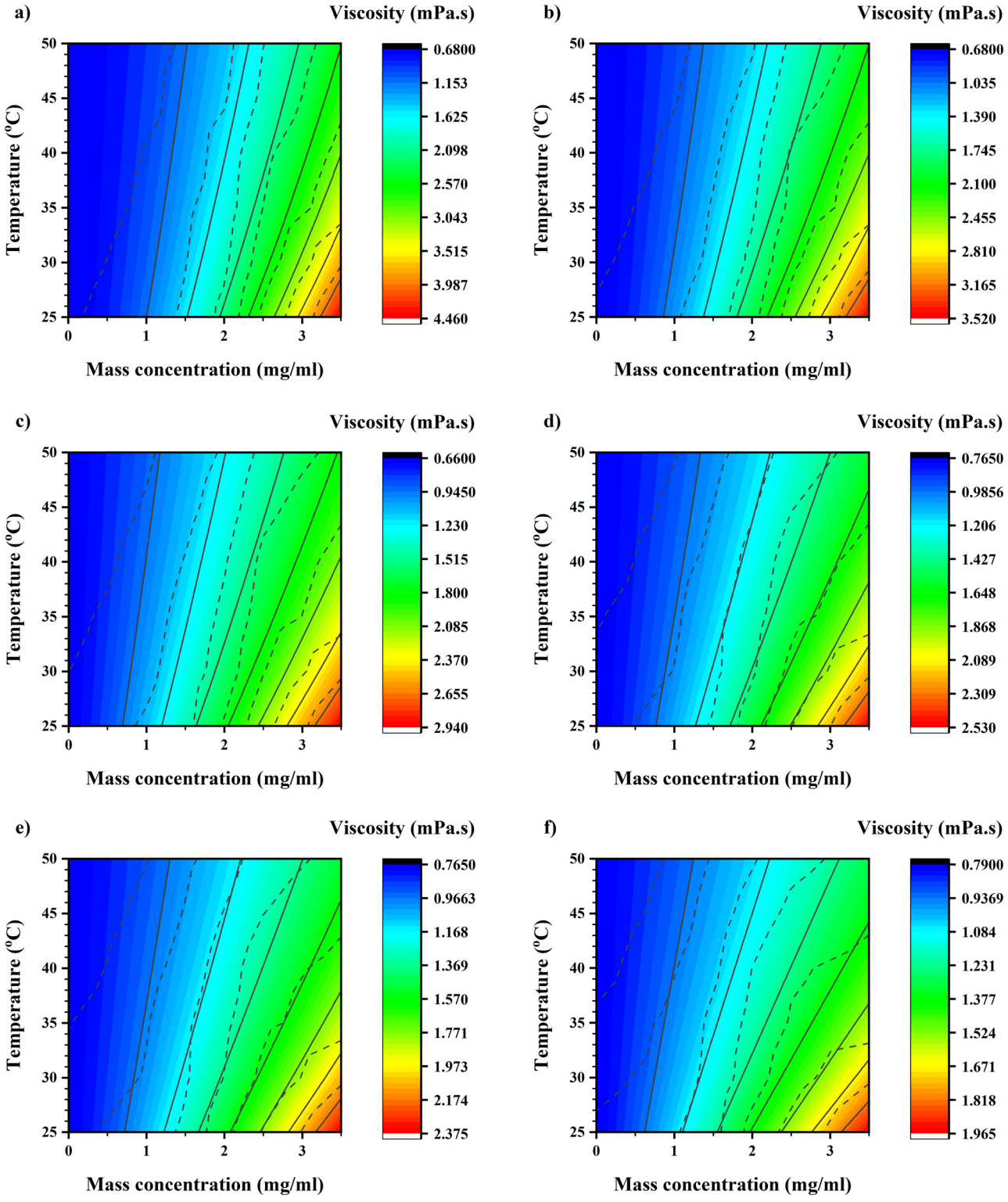

Figure 18: Main outcome (dashed lines) and trained outcome (solid lines) contour at (a) 10, (b) 20, (c) 30, (d) 50, (e) 60, and (f) 100 RPM.

gained in non-modeled temperature, SR, and wt%. The optimum hidden neurons number is 2/3 the size of the input layer plus the size of the output layer. Equations (12) and (13) are the ANN equations set on the empirical viscosity data.

For 12.23 s^{-1}:

$$\begin{aligned}\text{Vis} = {} & 0.61638 + 0.8301 * \exp(-0.5 \\ & * \text{pow}((\log(\text{wt}/4.03049)/(-0.4398)),2)) \\ & + 2.25745 * \exp(-0.5 * \text{pow}((\log((T/T_0) \\ & /0.10084)/1.45263),2)) + 7.78167 * \\ & \times \exp\left(-0.5 * \begin{pmatrix}\text{pow}((\log(\text{wt}/4.03049)/(-0.4398)),2) + \\ \text{pow}((\log((T/T_0)/0.10084)/1.45263),2)\end{pmatrix}\right),\end{aligned} \tag{12}$$

***R*-square: 0.9999.**

And for 122.3 s^{-1}:

$$\begin{aligned}\text{Vis} = {} & 16.00977 + (-18.16831) * \exp(-0.5 \\ & * \text{pow}((\log(\text{wt}/(5.53936 \times 10^{-10})) \\ & /(-37.41451)),2)) + 40.73228 * \\ & \times \exp(-0.5 * \text{pow}((\log((T/T_0)/0.48682)/0.95364),2)) \\ & + (-47.22344) \\ & * \exp\left(-0.5 * \begin{pmatrix}\text{pow}((\log(\text{wt}/(5.53936 \times 10^{-10})) \\ /(-37.41451)),2)+ \\ \text{pow}((\log((T/T_0)/0.48682)/0.95364),2)\end{pmatrix}\right),\end{aligned} \tag{13}$$

***R*-square: 0.9999.**

where "*T*" and "*wt*" are temperature and mass concentration, respectively, "T_0" is 25°C, and viscosity is in centipoise [71].

4 Conclusion

In this research, graphene, a two-dimensional material, was produced *via* the top-down technique while a homogeneous and stable nanofluid was made. Then, graphene–water nanofluid dynamic viscosity at a temperature range of 25–50°C and mass concentration range of 1.0–3.5 mg/mL was measured. Newtonian behavior appeared in the base fluid, but though graphene was dispersed in DW, nanofluid demonstrated the non-Newtonian (pseudoplastic behavior).

Viscosity shifts the flow features of a liquid which is a primary factor in demonstrating forces that should be overcome when fluids are transported in pipelines or employed in lubrication. Thus, the following results conclude which temperature and which concentration should be used:

- For 1.0 mg/mL nanofluid, from 25–50°C at 10 RPM, viscosity decreased by 56.9% and at 100 RPM, viscosity decreased by 42.5%.
- For 2.0 mg/mL nanofluid, from 25–50°C at 10 RPM, viscosity decreased by 54.9% and at 100 RPM, viscosity decreased by 42.3%.
- For 3.5 mg/mL nanofluid, from 25–50°C at 10 RPM, viscosity decreased by 38.5% and at 100 RPM, viscosity decreased by 33.3%.

Finally, the simple and reliable equations that can predict the rheological behavior of graphene/water nanofluid are calculated with $\boldsymbol{R^2}$ = 0.99 (deviation).

For future works, the viscosity of other carbon-based materials instead of graphene can be compared with this study. Also, the water can be replaced by oil, ethylene glycol, propylene glycol, *etc*., and the results can be compared with this work.

Acknowledgments: The authors are thankful to the Deanship of Scientific Research at Najran University for funding this work under the Research Collaboration Funding program grant code (NU/RC/SERC/11/9). Also, the authors gratefully acknowledge financial support from the German Research Foundation (DFG).

Funding information: Research funded by the Deanship of Scientific Research at Najran University under the Research Collaboration Funding program grant code (NU/RC/SERC/11/9). Also, the authors gratefully acknowledge financial support from the German Research Foundation (DFG).

Author contributions: All authors have accepted responsibility for the entire content of this manuscript and approved its submission.

Conflict of interest: The authors state no conflict of interest.

References

[1] Said Z, Hachicha AA, Aberoumand S, Yousef BA, Sayed ET, Bellos E. Recent advances on nanofluids for low to medium temperature solar collectors: energy, exergy, economic analysis and environmental impact. Prog Energy Combust Sci. 2021;84:100898. doi: 10.1016/j.pecs.2020.100898.

[2] Asadi A, Aberoumand S, Moradikazerouni A, Pourfattah F, Żyła G, Estellé P, et al. Recent advances in preparation methods and thermophysical properties of oil-based nanofluids: A state-of-the-art review. Powder Technol. 2019;352:209–26. doi: 10.1016/j.powtec.2019.04.054.

[3] Chu YM, Nazir U, Sohail M, Selim MM, Lee JR. Enhancement in thermal energy and solute particles using hybrid nanoparticles by engaging activation energy and chemical reaction over a parabolic surface *via* finite element approach. Fractal Fract. 2021;5(3):119. doi: 10.3390/fractalfract5030119.

[4] Alqaed S, Mustafa J, Sharifpur M, Cheraghian G. Using nanoparticles in solar collector to enhance solar-assisted hot process stream usefulness. Sustain Energy Technol Assess. 2022;52(4):101992. doi: 10.1016/j.seta.2022.101992.
[5] Almehmadi FA, Alqaed S, Mustafa J, Jamil B, Sharifpur M. Combining an active method and a passive method in cooling lithium-ion batteries and using the generated heat in heating a residential unit. J Energy Storage. 2022;49:104181. doi: 10.1016/j.est.2022.104181.
[6] Ma M, Zhai Y, Yao P, Li Y, Wang H. Synergistic mechanism of thermal conductivity enhancement and economic analysis of hybrid nanofluids. Powder Technol. 2020;373:702–15. doi: 10.1016/j.powtec.2020.07.020.
[7] Mustafa J, Almehmadi FA, Alqaed S. A novel study to examine dependency of indoor temperature and PCM to reduce energy consumption in buildings. J Build Eng. 2022;51(6):104249.
[8] Alqaed S, Mustafa J, Almehmadi FA. The effect of using phase change materials in a solar wall on the number of times of air conditioning per hour during day and night in different thicknesses of the solar wall. J Build Eng. 2022;51(A):104227.
[9] Cakmak NK, Said Z, Sundar LS, Ali ZM, Tiwari AK. Preparation, characterization, stability, and thermal conductivity of rGO-Fe_3O_4-TiO_2 hybrid nanofluid: An experimental study. Powder Technol. 2020;372:235–45. doi: 10.1016/j.powtec.2020.06.012.
[10] Mustafa J, Alqaed S, Sharifpur M. Incorporating nano-scale material in solar system to reduce domestic hot water energy demand. Sustain Energy Technol Assess. 2022;49(3):101735.
[11] Amirahmad A, Maglad AM, Mustafa J, Cheraghian G. Loading PCM into buildings envelope to decrease heat gain-performing transient thermal analysis on nanofluid filled solar system. Front Energy Res. 2021;9:727011.
[12] Bretado-de los Rios MS, Rivera-Solorio CI, Nigam KD. An overview of sustainability of heat exchangers and solar thermal applications with nanofluids: A review. Renew Sustain Energy Rev. 2021;142:110855. doi: 10.1016/j.rser.2021.110855.
[13] Ma J, Shahsavar A, Al-Rashed AA, Karimipour A, Yarmand H, Rostami S. Viscosity, cloud point, freezing point and flash point of zinc oxide/SAE50 nanolubricant. J Mol Liq. 2020;298:112045. doi: 10.1016/j.molliq.2019.112045.
[14] Nazeer M, Hussain F, Khan MI, El-Zahar ER, Chu YM, Malik MY. Theoretical study of MHD electro-osmotically flow of third-grade fluid in micro channel. Appl Math Comput. 2022;420:126868. doi: 10.1016/j.amc.2021.126868.
[15] Chu YM, Shankaralingappa BM, Gireesha BJ, Alzahrani F, Khan MI, Khan SU. Combined impact of Cattaneo-Christov double diffusion and radiative heat flux on bio-convective flow of Maxwell liquid configured by a stretched nano-material surface. Appl Math Comput. 2022;419:126883. doi: 10.1016/j.amc.2021.126883.
[16] Wang F, Khan MN, Ahmad I, Ahmad H, Abu-Zinadah H, Chu YM. Numerical solution of traveling waves in chemical kinetics: time-fractional fishers equations. Fractals. 2022;2240051. doi: 10.1142/S0218348X22400515.
[17] Alsarraf J, Shahsavar A, Khaki M, Ranjbarzadeh R, Karimipour A, Afrand M. Numerical investigation on the effect of four constant temperature pipes on natural cooling of electronic heat sink by nanofluids: a multifunctional optimization. Adv Powder Technol. 2020;31(1):416–32. doi: 10.1016/j.apt.2019.10.035.
[18] Niknejadi M, Afrand M, Karimipour A, Shahsavar A, Isfahani AH. Experimental investigation of the hydrothermal aspects of water–Fe_3O_4 nanofluid inside a twisted tube. J Therm Anal Calorim. 2020;143:1–10. doi: 10.1007/s10973-020-09271-0.
[19] Mustafa J, Alqaed S, Kalbasi R. Challenging of using CuO nanoparticles in a flat plate solar collector- Energy saving in a solar-assisted hot process stream. J Taiwan Inst Chem Eng. 2021;124(2):258–65.
[20] Ashraf A, Shafi WK, Ul Haq MI, Raina A. Dispersion stability of nano additives in lubricating oils–an overview of mechanisms, theories and methodologies. Tribol-Mater Surf Interfaces. 2022;16(1):34–56. doi: 10.1080/17515831.2021.1981720.
[21] Gulzar O, Qayoum A, Gupta R. Experimental study on stability and rheological behaviour of hybrid Al_2O_3-TiO_2 Therminol-55 nanofluids for concentrating solar collectors. Powder Technol. 2019;352:436–44, https://www.sciencedirect.com/science/article/abs/pii/S0032591019303080.
[22] Anand R, Raina A, Irfan Ul Haq M, Mir MJ, Gulzar O, Wani MF. Synergism of TiO_2 and graphene as nano-additives in bio-based cutting fluid – An experimental investigation. Tribol Trans. 2021;64(2):350–66. doi: 10.1080/10402004.2020.1842953.
[23] Alshayji A, Asadi A, Alarifi IM. On the heat transfer effectiveness and pumping power assessment of a diamond-water nanofluid based on thermophysical properties: an experimental study. Powder Technol. 2020;373:397–410. doi: 10.1016/j.powtec.2020.06.068.
[24] Maghrabie HM, Attalla M, Mohsen AA. Performance assessment of a shell and helically coiled tube heat exchanger with variable orientations utilizing different nanofluids. Appl Therm Eng. 2021;182:116013. doi: 10.1016/j.applthermaleng.2020.116013.
[25] Alagumalai A, Qin C, Vimal KE, Solomin E, Yang L, Zhang P, et al. Conceptual analysis framework development to understand barriers of nanofluid commercialization. Nano Energy. 2022;92:106736. doi: 10.1016/j.nanoen.2021.106736.
[26] Yan SR, Kalbasi R, Nguyen Q, Karimipour A. Rheological behavior of hybrid MWCNTs-TiO_2/EG nanofluid: a comprehensive modeling and experimental study. J Mol Liq. 2020;308:113058. doi: 10.1016/j.molliq.2020.113058.
[27] Tian XX, Kalbasi R, Jahanshahi R, Qi C, Huang HL, Rostami S. Competition between intermolecular forces of adhesion and cohesion in the presence of Graphene nanoparticles: Investigation of Graphene nanosheets/ethylene glycol surface tension. J Mol Liq. 2020;311:113329. doi: 10.1016/j.molliq.2020.113329.
[28] Chen J, Li Y, Huang L, Li C, Shi G. High-yield preparation of Graphene oxide from small graphite flakes *via* an improved Hummers method with a simple purification process. Carbon. 2015;81:826–34. doi: 10.1016/j.carbon.2014.10.033.
[29] Fu C, Zhao G, Zhang H, Li S. Evaluation and characterization of reduced Graphene oxide nanosheets as anode materials for lithium-ion batteries. Int J Electrochem Sci. 2013;8(5):6269–80.
[30] Alam SN, Sharma N, Kumar L. Synthesis of Graphene oxide (GO) by modified hummers method and its thermal reduction to obtain reduced Graphene oxide (rGO). Graphene. 2017;6(1):1–18. doi: 10.4236/Graphene.2017.61001.

[31] Aghahadi MH, Niknejadi M, Toghraie D. An experimental study on the rheological behavior of hybrid Tungsten oxide (WO_3)-MWCNTs/engine oil Newtonian nanofluids. J Mol Structure. 2019;1197:497–507. doi: 10.1016/j.molstruc.2019.07.080.

[32] Esfe MH, Rostamian SH. Rheological behavior characteristics of MWCNT-TiO_2/EG (40%–60%) hybrid nanofluid affected by temperature, concentration, and shear rate: An experimental and statistical study and a neural network simulating. Phys A Stat Mech Its Appl. 2020;553:124061. doi: 10.1016/j.physa.2019.124061.

[33] Kazemi I, Sefid M, Afrand M. A novel comparative experimental study on rheological behavior of mono & hybrid nanofluids concerned Graphene and silica nano-powders: characterization, stability and viscosity measurements. Powder Technol. 2020;366:216–29. doi: 10.1016/j.powtec.2020.02.010.

[34] Ma M, Zhai Y, Yao P, Li Y, Wang H. Effect of surfactant on the rheological behavior and thermophysical properties of hybrid nanofluids. Powder Technol. 2021;379:373–83. doi: 10.1016/j.powtec.2020.10.089.

[35] Lee J, Chen Y, Liang H, Kim S. Temperature-dependent rheological behavior of nanofluids rich in carbon-based nanoparticles. J Mol Liq. 2021;325:114659. doi: 10.1016/j.molliq.2020.114659.

[36] Dalkılıç AS, Açıkgöz Ö, Küçükyıldırım BO, Eker AA, Lüleci B, Jumpholkul C, et al. Experimental investigation on the viscosity characteristics of water based SiO_2-graphite hybrid nanofluids. Int Commun Heat Mass Transf. 2018;97:30–8. doi: 10.1016/j.icheatmasstransfer.2018.07.007.

[37] Sekhar YR, Sharma KV. Study of viscosity and specific heat capacity characteristics of water-based Al_2O_3 nanofluids at low particle concentrations. J Exp Nanosci. 2015;10(2):86–102. doi: 10.1080/17458080.2013.796595.

[38] Bahrami M, Akbari M, Karimipour A, Afrand M. An experimental study on rheological behavior of hybrid nanofluids made of iron and copper oxide in a binary mixture of water and ethylene glycol: non-Newtonian behavior . Exp Therm Fluid Sci. 2016;79:231–7. doi: 10.1016/j.expthermflusci.2016.07.015.

[39] Zhao TH, Khan MI, Chu YM. Artificial neural networking (ANN) analysis for heat and entropy generation in flow of non-Newtonian fluid between two rotating disks. Math Methods Appl Sci. 2021. doi: 10.1002/mma.7310.

[40] Afrand M, Nadooshan AA, Hassani M, Yarmand H, Dahari M. Predicting the viscosity of multi-walled carbon nanotubes/water nanofluid by developing an optimal artificial neural network based on experimental data. Int Commun Heat Mass Transf. 2016;77:49–53. doi: 10.1016/j.icheatmasstransfer.2016.07.008.

[41] Nguyen Q, Ghorbani P, Bagherzadeh SA, Malekahmadi O, Karimipour A. Performance of joined artificial neural network and genetic algorithm to study the effect of temperature and mass fraction of nanoparticles dispersed in ethanol. Math Methods Appl Sci. 2020. doi: 10.1002/mma.6688.

[42] Shahsavar A, Khanmohammadi S, Afrand M, Goldanlou AS, Rosatami S. On evaluation of magnetic field effect on the formation of nanoparticles clusters inside aqueous magnetite nanofluid: An experimental study and comprehensive modeling. J Mol Liq. 2020;312:113378. doi: 10.1016/j.molliq.2020.113378.

[43] Çolak AB. A novel comparative analysis between the experimental and numeric methods on viscosity of zirconium oxide nanofluid: Developing optimal artificial neural network and new mathematical model. Powder Technol. 2021;381:338–51. doi: 10.1016/j.powtec.2020.12.053.

[44] Sodeifian G, Niazi Z. Prediction of CO_2 absorption by nanofluids using artificial neural network modeling. Int Commun Heat Mass Transf. 2021;123:105193. doi: 10.1016/j.icheatmasstransfer.2021.105193.

[45] Wahab A, Khan MA, Hassan A. Impact of Graphene nanofluid and phase change material on hybrid photovoltaic thermal system: Exergy analysis. J Clean Prod. 2020;277:123370. doi: 10.1016/j.jclepro.2020.123370.

[46] Zheng Y, Zhang X, Shahsavar A, Nguyen Q, Rostami S. Experimental evaluating the rheological behavior of ethylene glycol under Graphene nanosheets loading. Powder Technol. 2020;367:788–95. doi: 10.1016/j.powtec.2020.04.039.

[47] Hamze S, Cabaleiro D, Maré T, Vigolo B, Estellé P. Shear flow behavior and dynamic viscosity of few-layer Graphene nanofluids based on propylene glycol-water mixture. J Mol Liq. 2020;316:113875. doi: 10.1016/j.molliq.2020.113875.

[48] Bakhtiari R, Kamkari B, Afrand M, Abdollahi A. Preparation of stable TiO_2-Graphene/Water hybrid nanofluids and development of a new correlation for thermal conductivity. Powder Technol. 2021;385:466–77. doi: 10.1016/j.powtec.2021.03.010.

[49] Nadooshan AA, Eshgarf H, Afrand M. Measuring the viscosity of Fe_3O_4-MWCNTs/EG hybrid nanofluid for evaluation of thermal efficiency: Newtonian and non-Newtonian behavior. J Mol Liq. 2018;253:169–77. doi: 10.1016/j.molliq.2018.01.012.

[50] Malekahmadi O, Kalantar M, Nouri-Khezrabad M. Effect of carbon nanotubes on the thermal conductivity enhancement of synthesized hydroxyapatite filled with water for dental applications: experimental characterization and numerical study. J Therm Anal Calorim. 2021;144(6):2109–26. doi: 10.1007/s10973-021-10593-w.

[51] Shahsavani E, Afrand M, Kalbasi R. Experimental study on rheological behavior of water–ethylene glycol mixture in the presence of functionalized multi-walled carbon nanotubes. J Therm Anal Calorim. 2018;131(2):1177–85. doi: 10.1007/s10973-017-6711-8.

[52] Abidi A, Jokar Z, Allahyari S, Sadigh FK, Sajadi SM, Firouzi P, et al. Improve thermal performance of Simulated-Body-Fluid as a solution with an ion concentration close to human blood plasma, by additive Zinc Oxide and its composites: ZnO/Carbon Nanotube and ZnO/Hydroxyapatite. J Mol Liq. 2021;342:117457. doi: 10.1016/j.molliq.2021.117457.

[53] Ibrahim M, Saeed T, Chu, YM, Ali HM, Cheraghian G, Kalbasi R. Comprehensive study concerned graphene nano-sheets dispersed in ethylene glycol: Experimental study and theoretical prediction of thermal conductivity. Powder Technol. 2021;386(9):51–9. doi: 10.1016/j.powtec.2021.03.028.

[54] García A, Culebras M, Collins MN, Leahy JJ. Stability and rheological study of sodium carboxymethyl cellulose and alginate suspensions as binders for lithium ion batteries. J Appl Polym Sci. 2018;135(17):46217. doi: 10.1002/app.46217.

[55] Phuoc TX, Massoudi M, Chen RH. Viscosity and thermal conductivity of nanofluids containing multi-walled carbon nanotubes stabilized by chitosan. Int J Therm Sci. 2011;50(1):12–8. doi: 10.1016/j.ijthermalsci.2010.09.008.

[56] Shahsavar A, Salimpour MR, Saghafian M, Shafii MB. Effect of magnetic field on thermal conductivity and viscosity of a magnetic nanofluid loaded with carbon nanotubes. J Mech Sci Technol. 2016;30(2):809–15. doi: 10.1007/s12206-016-0135-4.
[57] Alsarraf J, Malekahmadi O, Karimipour A, Tlili I, Karimipour A, Ghashang M. Increase thermal conductivity of aqueous mixture by additives Graphene nanoparticles in water *via* an experimental/numerical study: Synthesise, characterization, conductivity measurement, and neural network modeling. Int Commun Heat Mass Transf. 2020;118:104864. doi: 10.1016/j.icheatmasstransfer.2020.104864.
[58] Sun C, Taherifar S, Malekahmadi O, Karimipour A, Karimipour A, Bach QV. Liquid paraffin thermal conductivity with additives tungsten trioxide nanoparticles: synthesis and propose a new composed approach of fuzzy logic/artificial neural network. Arab J Sci Eng. 2021;46:2543–52. doi: 10.1007/s13369-020-05151-9.
[59] Bhattacharjee S. DLS and zeta potential–what they are and what they are not? J Controlled Rel. 2016;235:337–51. doi: 10.1016/j.jconrel.2016.06.017.
[60] ASHRAE. 2015 Ashrae handbook; 2015.
[61] Jeong J, Li C, Kwon Y, Lee J, Kim SH, Yun R. Particle shape effect on the viscosity and thermal conductivity of ZnO nanofluids. Int J Refrig. 2013;36(8):2233–41. doi: 10.1016/j.ijrefrig.2013.07.024.
[62] Namburu PK, Kulkarni DP, Misra D, Das DK. Viscosity of copper oxide nanoparticles dispersed in ethylene glycol and water mixture. Exp Therm Fluid Sci. 2007;32(2):397–402. doi: 10.1016/j.expthermflusci.2007.05.001.
[63] Sundar LS, Singh MK, Sousa AC. Investigation of thermal conductivity and viscosity of Fe_3O_4 nanofluid for heat transfer applications. Int Commun Heat Mass Transf. 2013;44:7–14. doi: 10.1016/j.icheatmasstransfer.2013.02.014.
[64] Yu W, Xie H, Chen L, Li Y. Investigation of thermal conductivity and viscosity of ethylene glycol based ZnO nanofluid. Thermochim Acta. 2009;491(1–2):92–6. doi: 10.1016/j.tca.2009.03.007.
[65] Bashirnezhad K, Bazri S, Safaei MR, Goodarzi M, Dahari M, Mahian O, et al. Viscosity of nanofluids: a review of recent experimental studies. Int Commun Heat Mass Transf. 2016;73:114–23. doi: https://doi.org/10.1016/j.icheatmasstransfer.2016.02.005.
[66] Ahammed N, Asirvatham LG, Wongwises S. Effect of volume concentration and temperature on viscosity and surface tension of Graphene–water nanofluid for heat transfer applications. J Therm Anal Calorim. 2016;123(2):1399–409. doi: 10.1007/s10973-015-5034-x.
[67] Khodadadi H, Toghraie D, Karimipour A. Effects of nanoparticles to present a statistical model for the viscosity of MgO-Water nanofluid. Powder Technol. 2019;342:166–80. doi: 10.1016/j.powtec.2018.09.076.
[68] Nguyen Q, Rizvandi R, Karimipour A, Malekahmadi O, Bach QV. A novel correlation to calculate thermal conductivity of aqueous hybrid graphene oxide/silicon dioxide nanofluid: synthesis, characterizations, preparation, and artificial neural network modeling. Arab J Sci Eng. 2020;45(11):9747–58. doi: 10.1007/s13369-020-04885-w.
[69] Karimipour A, Ghasemi S, Darvanjooghi MH, Abdollahi A. A new correlation for estimating the thermal conductivity and dynamic viscosity of CuO/liquid paraffin nanofluid using neural network method. Int Commun Heat Mass Transf. 2018;92:90–9. doi: 10.1016/j.icheatmasstransfer.2018.02.002.
[70] Shahsavar A, Khanmohammadi S, Karimipour A, Goodarzi M. A novel comprehensive experimental study concerned synthesizes and prepare liquid paraffin-Fe_3O_4 mixture to develop models for both thermal conductivity & viscosity: a new approach of GMDH type of neural network. Int J Heat Mass Transf. 2019;131:432–41. doi: 10.1016/j.ijheatmasstransfer.2018.11.069.
[71] Toghraie D, Sina N, Jolfaei NA, Hajian M, Afrand M. Designing an Artificial Neural Network (ANN) to predict the viscosity of Silver/Ethylene glycol nanofluid at different temperatures and volume fraction of nanoparticles. Phys A Stat Mech Appl. 2019;534:122142. doi: 10.1016/j.physa.2019.122142.
[72] Du C, Nguyen Q, Malekahmadi O, Mardani A, Jokar Z, Babadi E, et al. Thermal conductivity enhancement of nanofluid by adding multiwalled carbon nanotubes: Characterization and numerical modeling patterns. Math Methods Appl Sci. 2020. doi: 10.1002/mma.6466.
[73] Li Y, Moradi I, Kalantar M, Babadi E, Malekahmadi O, Mosavi A. Synthesis of new dihybrid nanofluid of TiO_2/MWCNT in water–ethylene glycol to improve mixture thermal performance: preparation, characterization, and a novel correlation *via* ANN based on orthogonal distance regression algorithm. J Therm Anal Calorim. 2021;144(6):2587–603. doi: 10.1007/s10973-020-10392-9.
[74] Karimipour A, Malekahmadi O, Karimipour A, Shahgholi M, Li Z. Thermal conductivity enhancement *via* synthesis produces a new hybrid mixture composed of copper oxide and multi-walled carbon nanotube dispersed in water: experimental characterization and artificial neural network modeling. Int J Thermophys. 2020;41(8):116. doi: 10.1007/s10765-020-02702-y.
[75] Jabbari F, Rajabpour A, Saedodin S. Viscosity of carbon nanotube/water nanofluid. J Therm Anal Calorim. 2019;135(3):1787–96. doi: 10.1007/s10973-018-7458-6.
[76] Cheraghian G, Afrand M. Nanotechnology for drilling operations. In Emerging nanotechnologies for renewable energy. Amsterdam, Netherlands: Elsevier; 2021. p. 135–48. doi: 10.1016/B978-0-12-821346-9.00008-0.
[77] Alqaed S, Almehmadi FA, Mustafa J, Husain S, Cheraghian G. Effect of nano phase change materials on the cooling process of a triangular lithium battery pack. J Energy Storage. 2022;51(9):104326. doi: 10.1016/j.est.2022.104326.